THE VARIABILITY AND SEASONAL CYCLE OF THE SOUTHERN OCEAN CARBON FLUX

A Thesis
Presented to
The Academic Faculty

by

Wei-Ching Hsu

In Partial Fulfillment
of the Requirements for the Degree
Master of Science in the
School of Earth and Atmospheric Sciences

Georgia Institute of Technology
August 2013

THE VARIABILITY AND SEASONAL CYCLE OF THE SOUTHERN OCEAN CARBON FLUX

Approved by:

Dr. Taka Ito, Advisor
School of Earth and Atmospheric Sciences
Georgia Institute of Technology

Dr. Emanuele Di Lorenzo
School of Earth and Atmospheric Sciences
Georgia Institute of Technology

Dr. Dan Jones
School of Earth and Atmospheric Sciences
Georgia Institute of Technology

Date Approved: June 24, 2013

ACKNOWLEDGEMENTS

First of all, I wish to thank my advisor Dr. Taka Ito, for the opportunity and support he gave me through out my master's study. Without him, I would never have managed to finish this thesis. I also want to thank Dr. Emanuele Di Lorenzo and Dr. Dan Jones for serving as my thesis reading committee and reviewing this thesis. Furthermore, I would like to thank our group member Dr. Dan Jones and Yohei Takano for fruitful discussion on research and their support on my life in the U.S. Special thanks go to my friends in both the U.S and Taiwan and my family, who gave me motivation for pursuing this degree.

TABLE OF CONTENTS

LIST OF FIGURES

SUMMARY

Both physical circulation and biogeochemical characteristics are unique in the Southern Ocean (SO) region, and are fundamentally different from those of the northern hemisphere. Moreover, according to previous research, the oceanic response to the trend of the Southern Annual Mode (SAM) has profound impacts on the future oceanic uptake of carbon dioxide in the SO. In other words, the climate and circulation of the SO are strongly coupled to the overlying atmospheric variability. However, while we have understanding on the SO physical circulation and have the ability to predict the future changes of the SO climate and physical processes, the link between the SO physical processes, the air-sea carbon flux, and correlated climate variability remains unknown. Even though scientists have been studying the spatial and temporal variability of the SO carbon flux and the associated biogeochemical processes, the spatial patterns and the magnitudes of the air-sea carbon flux do not agree between models and observations. Therefore, in this study, we utilized a modified version of a general circulation model (GCM) to performed realistic simulations of the SO carbon on seasonal to interannual timescales, and focused on the crucial physical and biogeochemical processes that control the carbon flux. The spatial pattern and the seasonal cycle of the air-sea carbon dioxide flux is calculated, and is broadly consistent with the climatological observations. The variability of air-sea carbon flux is mainly controlled by the gas exchange rate and the partial pressure of carbon dioxide (pCO_2), and the seasonal cycle of pCO_2 is in turn controlled by the compensating changes in temperature and dissolved inorganic carbon. We investigated the seasonal variability of dissolved inorganic carbon based on different

regional processes. Furthermore, we also investigated the dynamical adjustment of the surface carbon flux in response to the different gas exchange parameterizations, and conclude that parameterization has little impact on spatially integrated carbon flux. Our simulation well captured the SO carbon cycle variability on seasonal to interannual timescales, and we will improve our model by employ a better scheme of nutrient cycle, and consider more nutrients as well as ecological processes in our future study.

CHAPTER 1

INTRODUCTION

1.1 Climate and Circulation of the Southern Ocean

The climate and the circulation of the Southern Ocean (SO) fundamentally differ from those of the northern hemisphere because of variations in the land-sea distribution with profound implications on the climate variability and biogeochemical cycles of this region. Variability of the extratropical southern hemisphere atmosphere is dominated by the Antarctic Oscillation (AO) (Gong and Wang, 1998,1999; Wang, 1992), which is characterized by an alternation between the surface pressures of the mid and high latitudes (Gong and Wang, 1999). The spatial structure of the Southern Ocean is mostly zonally symmetric, reflecting the lack of major continents in the region. The intensity of AO can be measured by the Antarctic Oscillation Index (AOI), defined as the difference between the zonal mean sea level pressure values at 45°S and 65°S. Figure 1.1 shows the southern hemisphere sea level pressure pattern in JJA climatology. Thompson and

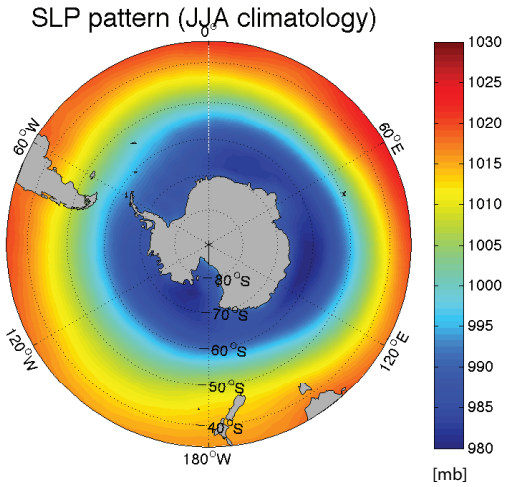

Figure 1-1: Southern Hemisphere JJA sea level pressure
(Data from SLP Monthly long term means, NCEP/NCAR Reanalysis)

Wallace (2000) defined the Southern Annular Mode (SAM), which captures the AO phenomenon, using the leading principal component of the 700 mb geopotential height south of 20°S in the atmosphere (Ciasto et al., 2008).

Both observational and modeling studies indicate that in recent decades the SAM index exhibits a positive multi-decadal trend. A positive SAM index is characterized by a lower polar cap geopotential height anomaly, an anomalously strong westerly wind, and cooling over Antarctica with the exception of the Antarctic Peninsula area (Thompson and Solomon, 2002). Thompson and Solomon (2002) showed a positive trend by analyzing the monthly mean radiosonde, the surface temperature, total column ozone, and the tropospheric geopotential height. Other observational studies show a similar trend in the SAM index [Visbeck, 2008; Renwick, 2004; Marshall, 2003]. The positive SAM trend during 1957 to 2012 is shown in figure 1.2.

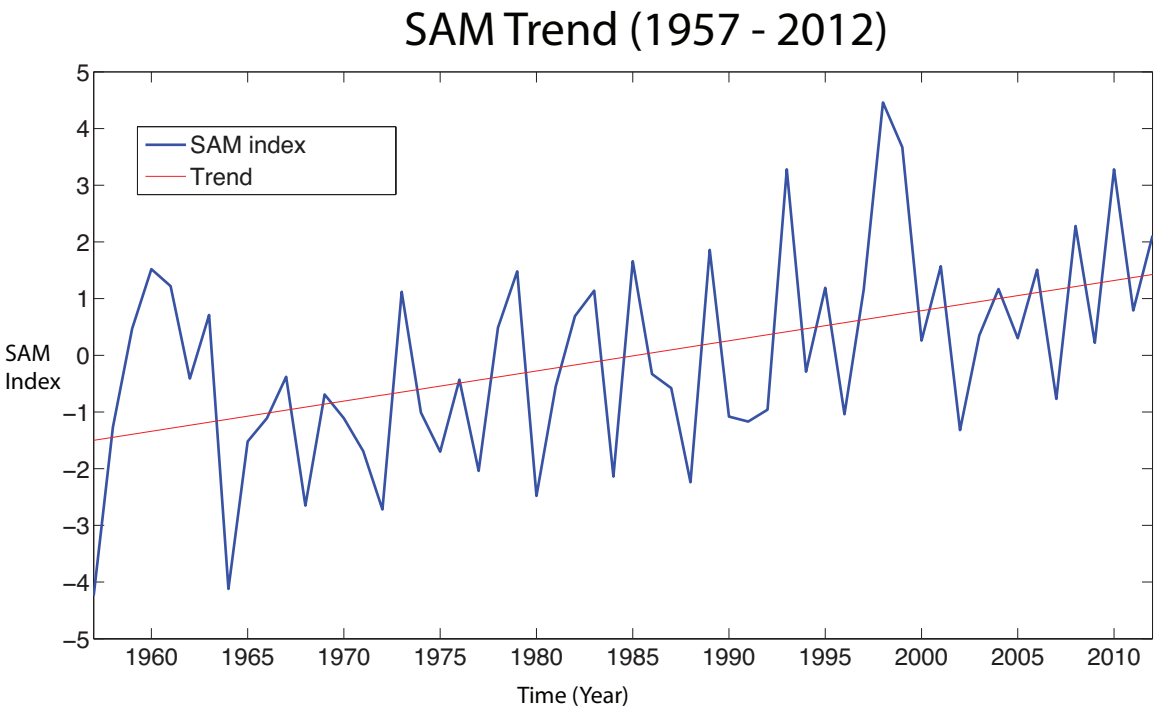

Figure 1-2: Annual SAM Index and the trend (1957 - 2012)
Data from: http://www.nerc-bas.ac.uk/icd/gjma/sam.html

Climate model simulations of the past several decades have also shown a positive SAM trend, in which the polar westerly wind has intensified and southward-shifted over the Antarctic Circumpolar Current (ACC) (Hall and Visbeck, 2002). The pattern of zonal wind variability has a dipole structure with an increase around 55°S and a decrease at about 35°S. In a positive SAM condition, at the latitude of the Drake Passage, equatorward Ekman transport that advects sea ice further north and induces an Ekman upwelling in the south of the circumpolar current increases. Gupta and England (2006) and Marini et al (2010) showed circulation changes under a positive SAM condition similar to those found by Hall and Visbeck (2002). Gupta and England (2006) further demonstrated the role of thermodynamic coupling between the ocean and the atmosphere whereby the ocean feeds back onto the atmosphere, increasing the persistence of SAM. These studies show that the Ekman upwelling intensifies in a positive SAM condition.

In a positive SAM condition, because of the uncertain degree of cancellation between the Ekman flow and eddy-induced circulation, we still do not thoroughly understand the behavior of the meridional overturning circulation (MOC) and the tilt of isopycnal surfaces. Tilted isopycnal surfaces of the SO are baroclinically unstable, spontaneously forming an energetic eddy field. Eddies have a tendency to homogenize potential vorticity and flatten isopycnal surfaces, counteracting the Ekman flow. To understand the compensation between the Ekman flow and eddy-induced circulation and the tilt of isopycnal surfaces, researchers have employed observation. Observed temperature and salinity changes based on ship- and float-based CTD data indicate that isopycnal surfaces are displaced downward while the tilt of density surfaces remain relatively constant (Böning et al., 2008). The tilt of density surfaces correlates with the transport of ACC. The density contrast across the ACC is directly related to the vertical shear of the zonal flow through the thermal wind balance. Assuming that deep current is relatively weak, overall ACC transport may also be proportional to the density gradient and the isopycnal tilt.

Fine-resolution models (e.g. Farneti and Delworth, 2010) also support the importance of wind-induced eddy fluxes and the insensitivity of the ACC mass transport to increased westerly wind stress. Using a scaling method, Meredith et al. (2012) argued that increased eddy activity itself cannot fully compensate for the increased Ekman flow within a reasonable dynamical range. Below a certain wind threshold, eddy activity will be too weak for compensation to occur, and MOC and the ACC then become strongly sensitive to changes in wind stress (Hofmann and Morales, 2011). Furthermore, because the characteristic time scale of isopycnal slope adjustment is many decades and centuries, detecting significant changes from a few decades of observations is difficult (Jones et al, 2011).

1.2 Southern Ocean Carbon Cycle

The SO has unique biogeochemical characteristics. Since the steep isopycnal slope directly connects the deep ocean carbon reservoir to the atmosphere, the SO is an important region for ocean carbon uptake. Annually, the global ocean absorbs about two petagrams of carbon, half of which occurs in south of 30°S (Takahashi et al., 2012; Khatiwala et al., 2009; Gruber et al., 2009). Air-sea carbon flux has been an area of intense research, and its pattern and magnitudes have been estimated by several methods: ocean in-situ observations (Takahashi et al., 2002, 2009; Manning and Keeling, 2006; Bender et al., 2005; Quay et al., 2003; Sabine et al., 2004), the inversion of general ocean circulation models (Gruber et al., 2009; Mikaloff Fletcher et al., 2006, 2007; Gloor et al., 2003), ocean forward models (OCMIP-2; Matear and Hirst , 1999), and atmospheric inverse models (Baker et al., 2006; Patra et al., 2006; Gurney et al., 2002, 2003, 2004). The estimates of these methods do not agree, particularly when the methods are applied to the SO. All estimates contain biases or errors that make a comparison of them valuable but challenging. For example, McNeil et al. (2007) indicated weaknesses of both the atmospheric inverse modeling and the pCO_2 observational predictions of air-sea

carbon flux. While atmospheric inverse modeling estimates are subject to biases resulting from unrealistic atmospheric transport and sparse regional record of the Southern Hemisphere, pCO_2 observations are subject to seasonal biases that result from difficulties in obtaining data during the austral winter.

Observational estimations can be further separated into several groups according to their method of measurement: the difference between sea and air pCO_2 (Takahashi et al., 2009), the mass balance of ^{13}C to ^{12}C (Quay et al., 2003), changes in atmospheric oxygen and CO_2 (Bender et al., 2005; Manning and Keeling, 2006), and changes in ocean CO_2 (Sabine et al., 2004). Since the net air-sea flux can be estimated by multiplying the gas transfer coefficients by the difference between the air and sea pCO_2 (ΔpCO_2) (Ho et al., 2011; Wanninkhof, 1992), this measurement is one of the primary methods for the direct measurement of the air-sea carbon flux (Takahashi et al., 2012). Takahashi et al. (2002) previously found an uptake region in the southern high latitudes, which was later corrected to be a moderate source. Figure 1.3 shows the annual-mean of

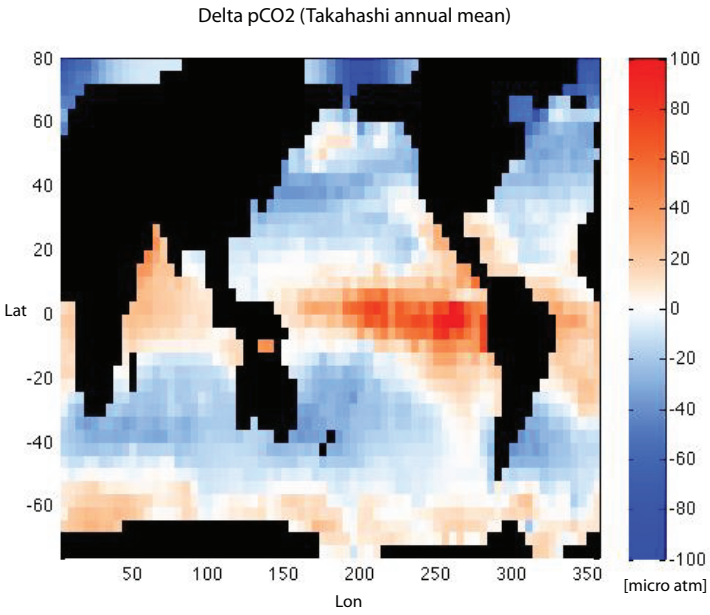

Figure 1-3: Takahashi global ΔpCO_2 annual mean
(Data from: http://www.ldeo.columbia.edu/res/pi/CO2/carbondioxide)

global ΔpCO_2 based on Takahashi (2010) observational dataset, which has a reference year of 2000. We can see positive ΔpCO_2 in high latitude SO, which indicates an outgassing of pCO_2 in the region. Moreover, negative ΔpCO_2 regions are shown in mid- to lower latitude SO. In a climatological sense, the mean CO_2 flux undergoes significant outgassing in the equatorial region (about 0.7 Pg C per year) counteracting the sinking of CO_2 in two major regions: around 40°N (about 0.7 Pg C per year) and around 40°S (about 1.0 Pg C per year) (Takahashi et al., 2009, 2012).

Takahashi et al. (2012) identified strong seasonal variability in the air-sea carbon flux with prominent sink for the global sea-air carbon budget centered around 40°S. During the austral summer, the biological drawdown of carbon contributes to a strong sink zone centered around 45°S. In higher latitude regions, the carbon flux is weak due to seasonal compensation between biological carbon uptake and CO_2 solubility caused by warming. During the austral winter, the spatial distribution of the air-sea carbon flux exhibits a pattern similar to that of the annual mean. The sink zone centered around 40°S is intensified by stronger wind and cooler seawater. Moreover, a strong CO_2 source zone is located around 60°S. The sea to air carbon flux in this zone is caused by the change of the ice field. However, this source zone makes a relatively small contribution to the annual carbon flux and the global sea-air CO_2 budget. The latitude-depend seasonal cycle of zonal-mean ΔpCO_2 based on Takahashi dataset is shown in figure 1.4.

Gruber et al. (2009) compared carbon flux estimates obtained by simulations of the inverse ocean model (Gruber et al., 2009; Mikaloff Fletcher et al., 2006, 2007) and measurements of the differences between air and sea pCO_2 (Takahashi et al., 2009). One of the advantages of ocean inversion is the separation of the natural and anthropogenic air-sea carbon flux. Similar to the study of Takahashi et al. (2009), Gruber et al. (2009) found a meridional distribution of air-sea carbon flux with outgassing in the tropics,

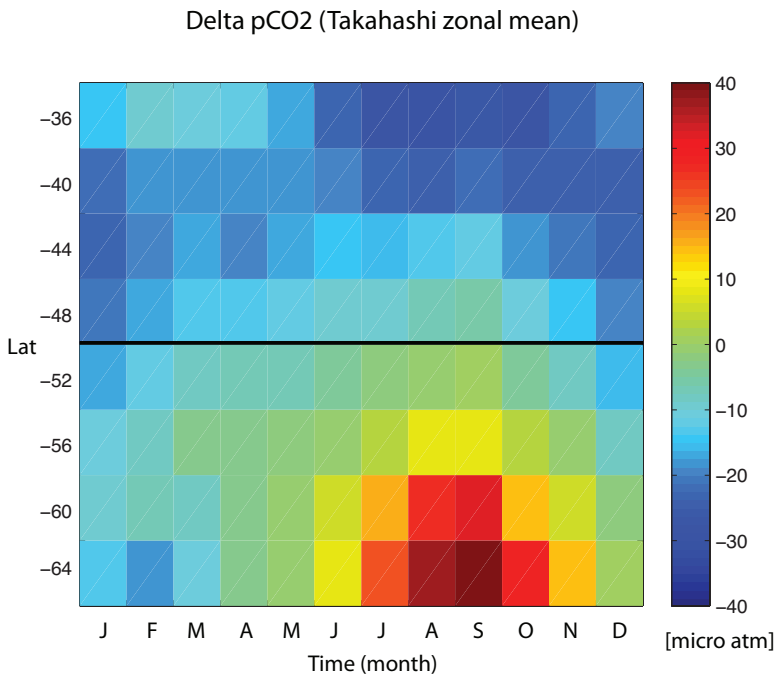

Figure 1-4: Seasonal cycle of latitudinal zonal-mean ΔpCO_2 (Data from: http://www.ldeo.columbia.edu/res/pi/CO2/carbondioxide)

sinking in the middle latitudes, and small fluxes in the high latitudes. Model simulations revealed strong compensation between the uptake of anthropogenic CO_2 and the outgassing of natural CO_2, and models and observations do not agree with regard to the pattern of ocean carbon uptake in the Southern Ocean. Estimates from ocean inversion models (Gruber et al., 2009) suggests more uniform carbon uptake while those from pCO_2-based observations show strong uptake in the mid-latitudes (44°S to 58°S) with a source in the high latitude region (south of 58°S)(Takahashi et al., 2009). To estimate the CO_2 uptake using surface dissolved inorganic carbon and total alkalinity, McNeil et al. (2007) also obtained a relatively uniform uptake region in the SO using an empirical approach.

As atmospheric CO_2 and the global climate change, the air-sea fluxes of both anthropogenic and natural CO_2 are predicted to change in the future (Yoshikawa et al., 2008; Gruber et al., 2004; Plattner et al., 2001; Matear and Hirst, 1999; Joos et al., 1999b; Sarmiento et al., 1998). Furthermore, Lenton and Matear (2007) and Lovenduski et al.

(2007) found a relationship between SAM and CO_2 flux in ocean biogeochemistry model simulations. They suggested that a decrease in ocean CO_2 sink resulting from the wind-driven upwelling of high-DIC waters from the deep ocean accompanies the positive SAM trend. Several studies show a similar weakening of the carbon sink under an increasing westerly wind. Le Quéré et al. (2007) showed an increase in deepwater upwelling with a stronger wind during between 1981 to 2004. Le Quéré et al. (2010) quantified the change in the difference between air and sea pCO_2 (20 μatm per decade), which is faster than the increase in atmospheric CO_2 (16 μatm per decade) between 1981 and 2007 using a biogeochemical ocean GCM. Takahashi et al. (2012) suggested that the observed pCO_2 in Antarctic surface waters has increased faster than atmospheric pCO_2, indicating a weakening of the carbon uptake.

1.3 Objective and Scope of This Study

The climate and circulation of the Southern Ocean is closely coupled to the overlying atmospheric variability. The oceanic response to the multi-decadal atmospheric trend has profound influences on the future carbon uptake in the SO. However, many questions remain about the processes controlling the air-sea carbon flux and its link to climate variability. The spatial patterns and magnitudes of modeled and observational estimates of carbon flux do not agree. Significant spatial and temporal variability exists in the carbon flux and associated biogeochemical processes (Lovenduski et al., 2008; Takahashi et al., 2009). Because of significant seasonal variability in temperature, wind, sea ice, and biological processes, the detection of relatively weak long-term trends is difficult (Takahashi et al., 2012). Furthermore, as the above processes undergo significant compensation in controlling the surface ocean pCO_2 and air-sea carbon fluxes, the interpretation of observations is also complex.

In this study, we perform realistic simulations of the SO carbon cycle on seasonal to interannual time scales, including the explicit representation of the mesoscale ocean

eddy fields. Therefore, we cannot directly address questions concerning long-term trends. Instead, we focus our attention on the key physical and biogeochemical processes that are crucial in controlling the behavior of the SO carbon sink. In particular, our model analysis will address the following two questions:

(1) What controls the variability and seasonal cycle of air-sea CO_2 flux in the SO?

(2) What are the relative roles of ocean transport, biological uptake, and air-sea CO_2 flux in regulating the regional carbon budget?

We will utilize a modified version of a general circulation model (GCM) to simulate the SO carbon flux on seasonal to interannual timescales based on a state estimate. The model we use in this study will be described in section two (methodology.) Then the analysis of the outputs will be discussed in the following section (results.) We started with answering the first question by concerning the contribution of different variables on the air-sea CO_2 flux variability. A detail about our simulations and analysis can be seen in section 3.1. To solve the second scientific question, we analyzed the regional carbon budget in the SO (section 3.2). Furthermore, in section 3.3, we conclude the results from section 3.1 and 3.2 to investigate the seasonal cycle of air-sea carbon flux in regional differences. We demonstrate the relationship between different variability by a schematic chart in the same section. After a brief summary in the results section, we have a conclusion and future work section to summarized this study and address some weakness of our study and possible future work.

CHAPTER 2

METHODOLOGY: MODEL DESCRIPTION

We used a numerical biogeochemistry model as a tool to better understand the variability of SO carbon flux on the seasonal to interannual time scales. The model is based on the SOSE-OCMIP model, in which a simple biogeochemistry scheme is coupled the Southern Ocean State Estimate (SOSE) (Woloszyn et al. 2011; Ito et al., 2010; Mazloff et al., 2010).

2.1 Southern Ocean State Estimate (SOSE)

The Southern Ocean State Estimate (SOSE) is a physical state estimate that combines an MIT general circulation model (Marshall et al., 1977) with observational data in the regional SO domain at an eddy-permitting resolution (Mazloff et al., 2010). Obeying the Navier-Stokes equations and conservation of mass, heat, and salt, the model is fitted to the data in a constrained least-squares sense. The observational dataset includes satellite SST data, Argo float profiles (Gould et al. 2004), CTD sections, satellite altimeter, and instrument-mounted seal profiles (Boehme et al. 2008). The model domain covers poleward of 25°S in the latitude-longitude grid of 1/6° horizontal resolution containing all. In the vertical direction, it has 42 varying thickness z-levels with a KPP mixed layer scheme (Large et al., 1994). A thermodynamical seaice scheme is also coupled to the model, and the exchanges of momentum, heat, and freshwater (salt) between the atmosphere and ocean are calculated by the bulk formulae (Large and Yeager, 2004).

To obtain the least squares fit to the suite of observational data, Mazloff et al. (2010) define the cost function as the weighted squared model state and data differences, which is summed over time and space. The same weighting has been used as the ECCO

global estimates (Forget and Wunsch, 2007; Ponte et al., 2007; Wunsch and Heimbach, 2007). To minimize the cost function, the gradients of cost function with respect to the control vector are calculated using an adjoint model (Giering and Kaminski, 1998). The control vector contains adjustable parameters of initial conditions (three-dimensional temperature and salinity) and boundary conditions (time varying two-dimensional atmospheric state.) The National Centers for Environmental Prediction–National Center for Atmospheric Research (NCEP–NCAR) reanalysis data (Kalnay et al., 1996) was used for the first-guess atmospheric state, and a special 1° global state estimate (Forget, 2010) was used for the first-guess initial condition and northern boundary conditions. The model state is iteratively optimized by the adjustment of the control vector according to the results of adjoint calculation. The quasi-Newton search algorithm of Gilbert and Lemare´chal (1989) was used for the gradient descent algorithm. After the cost function is reduced to an acceptable level, the adjusted control vector was used to run the free model forward in time to obtain the state estimate.

2.2 Biogeochemistry Model

We simulate the Southern Ocean carbon cycle in the offline mode based on the modified OCMIP-2 scheme (Ito et al., 2010; Woloszyn et al., 2011). The tracer transport is calculated using the five-day averaged state estimates from SOSE including the three-dimensional velocity fields, temperature, salinity, and the KPP mixing coefficients. The circulation and mixing fields are pre-computed, making the model simulation computationally efficient. The biogeochemistry model is based on the Ocean Carbon-Cycle Model Intercomparison Project phase two (OCMIP-2) scheme (Najjar et al., 1992), in which the near-surface (<75m) phosphate concentration is restored toward the monthly climatology using the linear relaxation if the simulated concentration was greater than that of climatology. The reference climatology was based on World Ocean Atlas 2009 (Garcia et al., 2010). Biological carbon uptake was then parameterized using the constant

stoichiometric ratios, which have the elemental ratio of organic material between phosphate, carbon and oxygen of 1:117:-170. One-third of this carbon uptake was directed to the sinking particulate pool, and the vertical dissolution for this pool was computed based on a power-law function, specifically, the Martin curve (Martin et al., 1987). To calculate the calcium carbonate formation, a uniform carbonate to organic rain ratio of 0.07 is used. We spun up the model for ten years from 1995 to 2004 by an initialization in 1995 based on the Global Ocean Data Analysis Project data set (GLODAP) (Key et al., 2004). We repeated the same annual cycles as those in 2005. For the simulation period of 2005 to 2008, the time-varying circulation fields and boundary conditions are used. The air-sea CO_2 flux is calculated using the ten meter wind speed based on the satellite scatterometer (QuikScat). Atmospheric pCO_2 is based on average monthly zonal mean values derived from GLOBALVIEW dataset (GLOBALVIEW-CO2, 2012) provided by NOAA ESRL.

Woloszyn et al (2011) compared an earlier version of SOSE-OCMIP simulations with several in-situ and observational datasets. Considering the annual mean of air-sea carbon flux in the Drake Passage, the model outputs are consistent with the Takahashi climatology (Takahashi et al., 2009), which has the annual mean referenced to 2000. Even though the simulated outgassing of carbon dioxide is stronger and equatorward shifted than that of observation, the model well captured the general spatial pattern and magnitudes, with a dominant outgassing region around 50°S to 60°S, and the main uptake region north of 50°S.

Woloszyn et al (2011) also made a comparison between the in-situ observations (CLIVAR repeat hydrography data from line A16S (25°W–40°W) and P16S (150°W)) and SOSE-OCMIP model simulations for the top 1000m. The model reproduced the observed pattern of temperature, salinity, alkalinity, and Dissolved Inorganic Carbon (DIC) with small misfits along the P16S line. Similarly, the model well reproduced all temperature, salinity, Alkalinity and DIC in Atlantic sector, with misfits even smaller

than those in Pacific region. In this study, we extend the simulation period to four years (2005-2009) using a newer version SOSE (iteration 59).

CHAPTER 3

RESULTS

3.1 Drivers of the Variability and Seasonal Cycle of Air-sea Carbon Flux

To investigate the variability of air-sea CO_2 flux in the SO, we started with the air-sea CO_2 flux equation, which is written as:

$$\mathrm{F_{CO2}} = (1\text{-}\mathrm{f_{ice}})\mathrm{GK_H}(\mathrm{pCO_2}^{\mathrm{ocn}}\text{-}\mathrm{pCO_2}^{\mathrm{atm}}),$$

where the air-sea flux (F_{CO2}) is proportional to the multiplier of gas exchange coefficient (G), Henry's law coefficient (K_H), and the difference of oceanic and atmospheric partial pressure of carbon dioxide ($pCO_2{}^{ocn} - pCO_2{}^{atm}$). $(1 - f_{ice})$ includes the effect of sea ice. The grids with fully covered sea ice have $f_{ice} = 1$, and those with no sea ice have $f_{ice} = 0$. In other words, sea ice slows down the air-sea flux. Note that Henry's law coefficient depends on temperature and salinity, which is based on the SOSE product. Having the typical range of temperature and salinity in the SO region, the solubility can decrease by about 60% by the temperature contribution (0 to 30°C) and decrease by 1.5% by the salinity contribution (34 to 37 psu). The atmospheric partial pressure of carbon dioxide is based on the observational dataset. While the model explicitly calculates the air-sea CO_2 fluxes including all these terms, we focused on the gas exchange rate and the oceanic pCO_2 variability that contributes to the seasonal to interannual variability of air-sea flux in the SO.

3.1.1 Control Simulation

Figure 3.1 shows the maps of the air-sea flux (F_{CO2}), gas exchange rate (G), and the oceanic partial pressure of carbon dioxide (pCO_2), based on their four-year time mean spatial patterns. Because of the constraint of the time period of our simulations, we

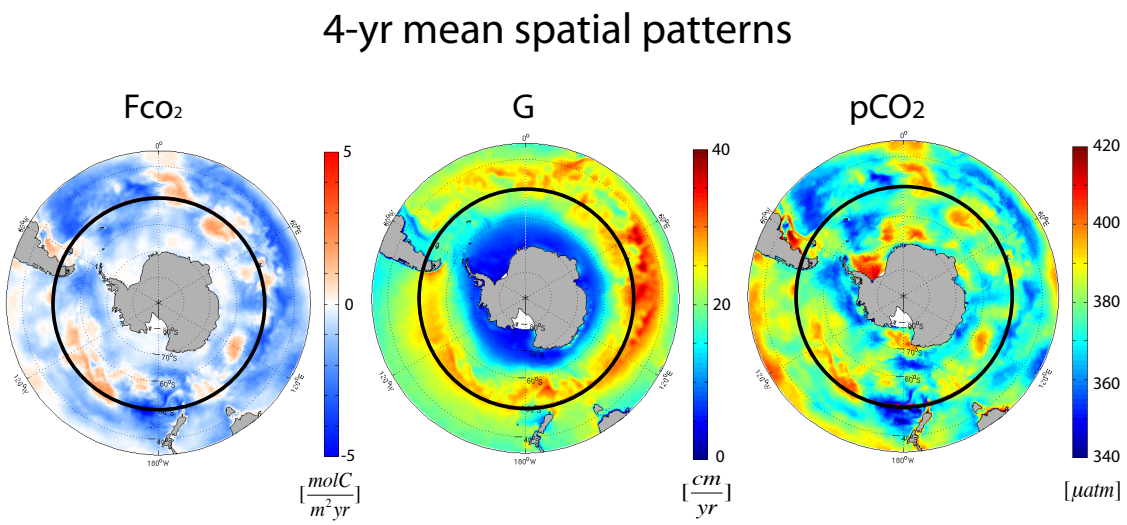

Figure 3-1: Four-year-mean special patterns of air-sea carbon flux, gas exchange rate, and oceanic partial pressure of carbon dioxide

calculated the "climatology" using the whole four-year (2005-2008) of the SOSE-OCMIP model outputs to demonstrate the patterns in interannual time scale.

In figure 3.1, we can see that G is very zonally symmetric, with smaller values in higher latitudes because of relatively small wind speed and lower temperature. (The black circle separating higher (Antarctic) and lower (Subantarctic) latitudes set at the 50°S latitudinal line.) In lower latitudes, the G magnitudes are higher, especially around 50°S. The pattern of F_{CO2} shows uptake regions in both higher latitudes and lower latitudes, while outgassing regions occur around mid-latitudes (~50°S). The pattern of pCO_2 is very similar to that of F_{CO2}. However, both pCO_2 and F_{CO2} patterns have are zonally asymmetric. Having the mean pCO_2^{atm} value about 380 ppm with little variances in both time and space, the signs of regional ($pCO_2^{ocn} - pCO_2^{atm}$) are matching with those of F_{CO2}.

Therefore, because of large latitudinal variances, we choose to separate the SO into two regions: the Antarctic and the Subantarctic regions. The Antarctic region is defined as 50°S to 78°S, while the Subantarctic region is defined as 35°S to 50°S of the SO in this study (Figure 3.2). We divided the SO by 50°S for two reasons: First, the

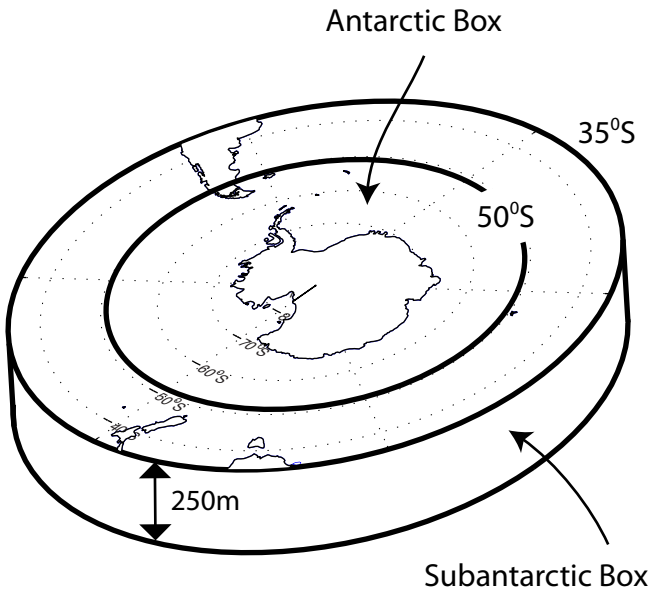

Figure 3-2: An illustration of the Antarctic and the Subantarctic regions

distributions of nutrient such as phosphate are zonally symmetric with a large gradient around 50°S; Second, The parameters associated with the carbon flux such as oceanic pCO_2, air-sea CO_2 flux and gas exchange rate have large gradient in the meridional direction.

Furthermore, to explain the reason why we have smaller G in higher latitudes, we can demonstrate the relationship between G and both temperature and wind speed using the equations of G. We used the gas exchange rate of Wanninkhof (1992) for our control runs, and both cubic and quadratic form of gas exchange rate from Ho et al. (2011) for perturbation runs. We performed sensitivity experiments to quantify uncertainty from parameterization of air-sea gas transfer. (In our simulations, surface DIC and pCO_2 dynamically adjust to the different gas exchange parameterization.) The expressions of the gas exchange rate (in $\frac{cm}{yr}$) are as follows:

$$G_{waQ} = 0.31 Wspd^2 \sqrt{\frac{660}{Sc}},$$

$$G_{hoQ} = 0.277 Wspd^2 \sqrt{\frac{600}{Sc}},$$

$$and \;\; G_{hoC} = 0.0241 Wspd^3 \sqrt{\frac{600}{Sc}},$$

where Sc is the Schmidt number, which depends on both temperature and salinity; Wspd is the ten-meter wind speed; G_{waQ}, G_{hoQ}, and G_{hoC} are the quadratic equation from Wanninkhof (1992), quadratic equation and cubic equation from Ho et al. (2011), respectively.

Figure 3.3 shows the relationship between G and temperature as well as wind

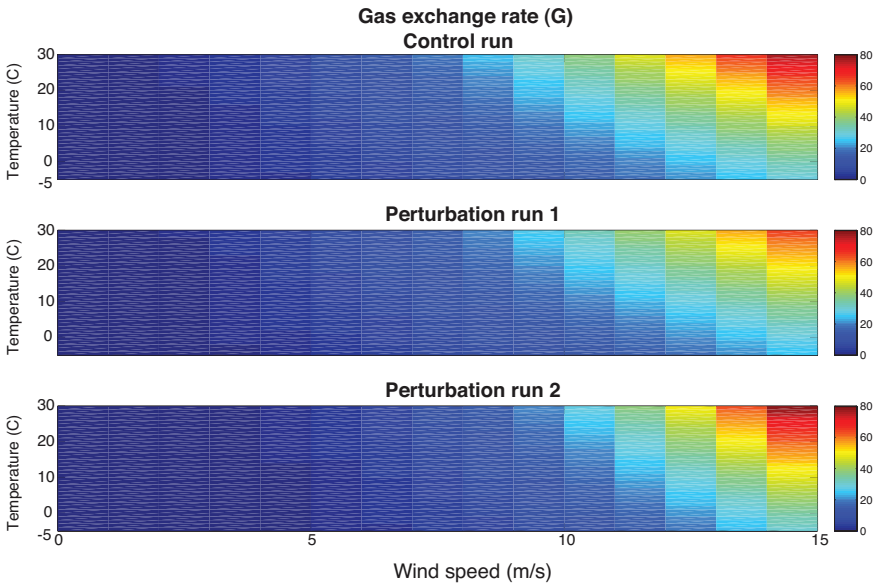

Figure 3-3: The relationship between the gas exchange rates, sea surface temperature (SOSE), and ten-meter wind speed (QuikScat)

speed using the three expressions of G (Wanninkhof, 1992 (the control run); Ho et al., 2011 (perturbation run 1 and 2 for quadratic and cubic equations, respectively)). An increase of G occurs with increasing in temperature and wind speed with different rates.

Note that we are only considering the control simulation (base line G: Wanninkhof (1992)) in figure 3.1.

3.1.2 Sensitivity Study on Air-sea Gas Exchange Rate

To calculate the sensitivity of the air-sea carbon flux to the gas exchange rate, we used three different expressions for G: Wanninkhof (1992) for our control simulations, both cubic and quadratic form of gas exchange rate from Ho et al. (2011) for our perturbation simulations. The time-mean spatial patterns of F_{CO2}, G, and pCO_2 from the two perturbation simulations (not shown) are similar to those from the control simulation. However, if we take the difference between three simulations quantitatively, regional differences occur (figure 3.4). The differences between the three simulations are smaller

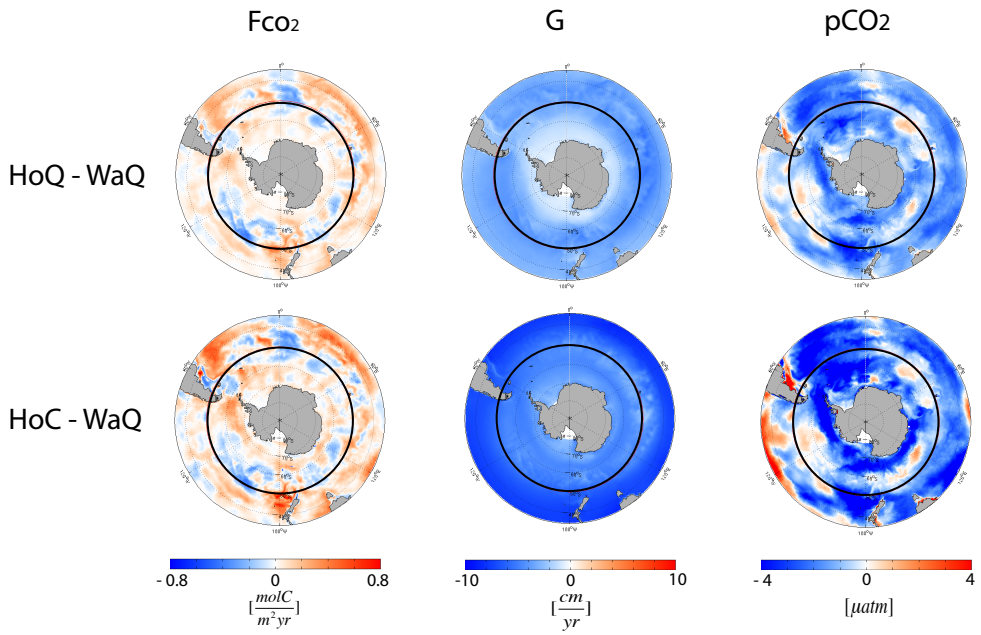

Figure 3-4: The regional differences of air-sea carbon flux, gas exchange rate, and oceanic partial pressure of carbon dioxide between the four-year mean of the perturbation simulations (HoQ and HoC, representing the quadratic and cubic expressions from Ho et al. (2011)) and that of the control simulation (WaQ, representing the quadratic expression from Wanninkhof (1992).)

than 0.8 $molC/m^2yr$ for F_{CO2}, which has a range of ±5 $molC/m^2yr$ in the SO region (figure 3.1). For G, the differences are in a range of ± 10 cm/yr, with the SO G values from 0 to 40 cm/yr. The differences of oceanic pCO_2 between the three simulations are in a range of ±4 μatm, while the four-year average of pCO_2 in the SO region is from 340 to 420 μatm. Here we used the control simulation as the basic patterns. Note that the differences are larger in the Subantarctic region but are with the same orders as those in the Antarctic region. This latitudinal difference may because of the effect of lower temperature, lower wind speed, and higher coverage of sea ice in higher latitudes.

Other than the time-mean spatial patterns, we also investigated the time variances of F_{CO2}, G, and pCO_2 (Figure 3.5, figure 3.6, and figure 3.7, respectively) using three

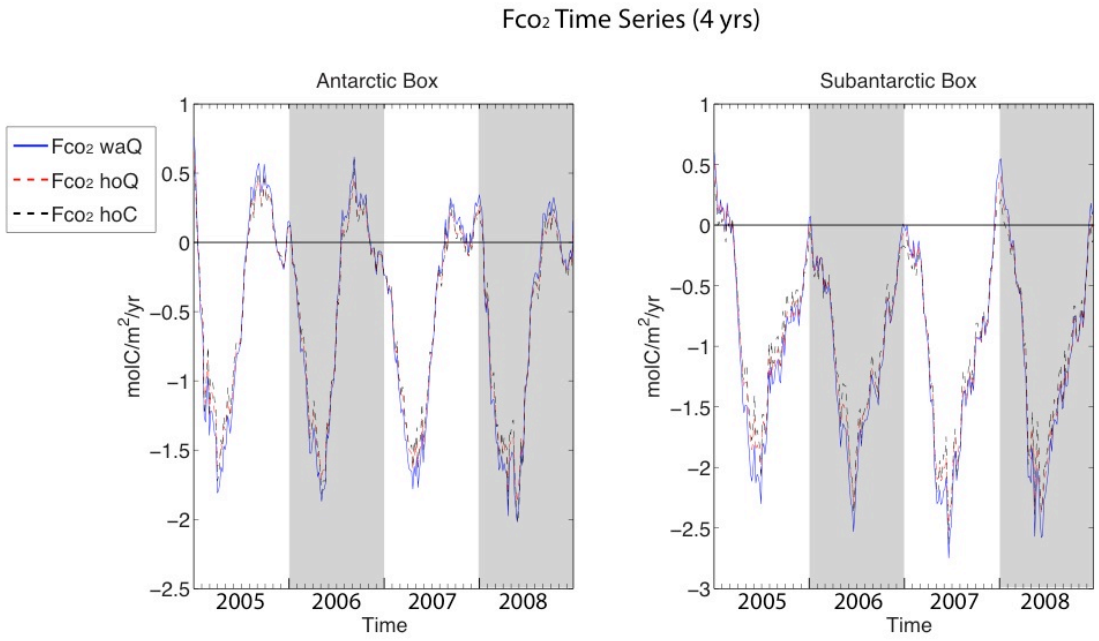

Figure 3-5: The time series of the regional mean of air-sea carbon flux based on different parameterization of the G

different expressions of G. Note that the variability of G and pCO_2 are two of the drivers that contribute to the variability of F_{CO2} in our simulations. For all three components, we see a large seasonality with a larger interannual variability in the Subantarctic region,

except the maximum G in the Antarctic region during summer to fall. The model simulates the three-dimensional distribution of biogeochemical tracers, surface pCO_2, and air-sea CO_2 fluxes, in conjunction with the parameterization of G. As a result, we will have different magnitudes of pCO_2 and F_{CO2} based on our paramerization of G.

Figure 3.6 shows that the interannual variability is not obvious in the time series of G, while the seasonality is large and especially in the Subantartic region. Note that

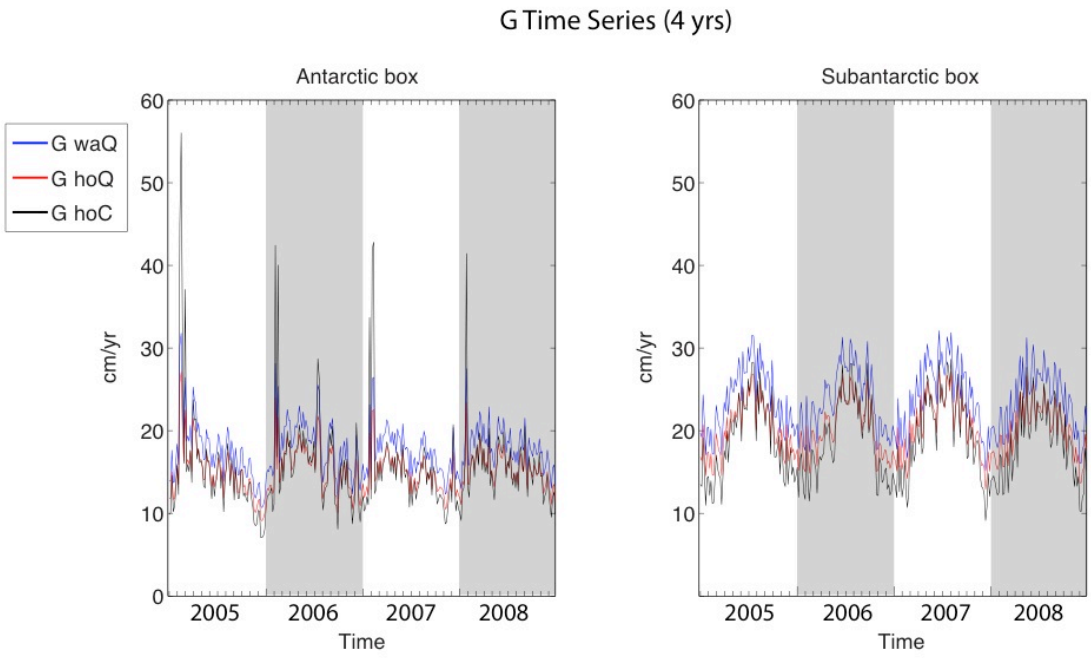

Figure 3-6: The time series of the regional mean of gas exchange rate based on different parameterization of G

there are some peaks in Antarctic region due to temporary large wind speed during late austral summer. Comparing figure 3.6 to figure 3.7, the maximum of G is corresponds to the minimum of pCO_2. However, the values of G only control the magnitudes of F_{CO2} but not the signs of it. Moreover, the time variability of pCO_2 (figure 3.7) shows a similarity with that of F_{CO2} (figure 3.5) in both seasonal and interannual time scales. Maximum uptake of carbon dioxide by the ocean happens during austral fall in Antarctic region, and during late fall to winter in Subantarctic region. On the other hand, maximum outgassing

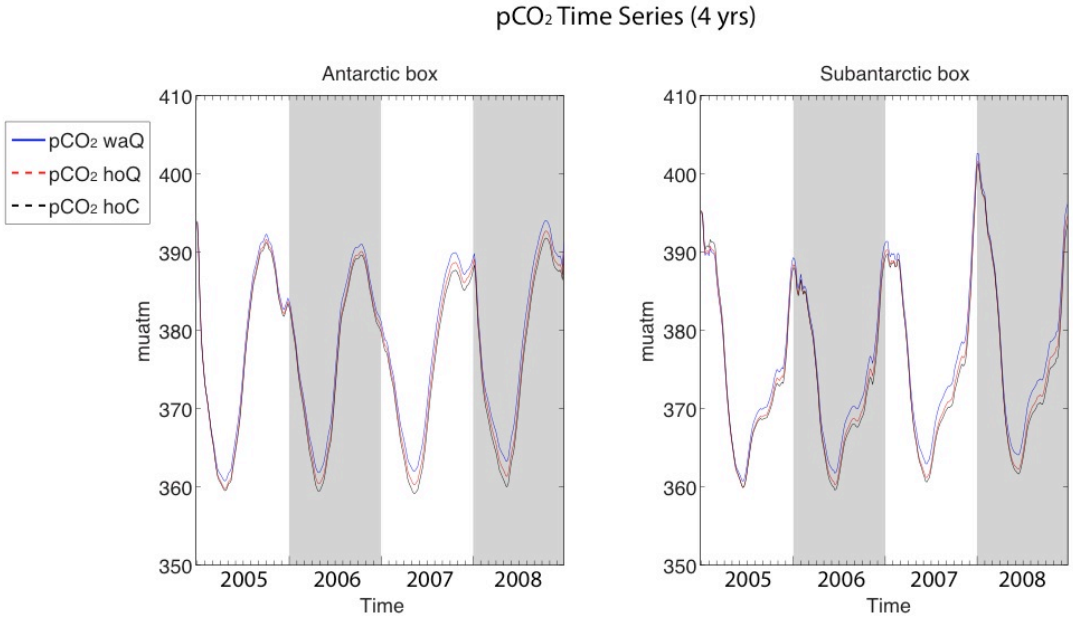

Figure 3-7: The time series of the regional mean of oceanic partial pressure of carbon dioxide based on different parameterization of G

in Antarctic region occurs during austral spring to summer, while that in Subantarctic region happens only in winter with much smaller magnitudes. Note that the magnitudes of uptake peaks are much larger than that of outgassing peaks, regardless of the region. Therefore, the seasonal variability of G reinforces the ocean carbon uptake from air-sea flux in both Antarctic and Subantarctic regions.

From regional average of pCO_2 and F_{CO2}, we see little differences between different parameterization of gas exchange rates. In other words, even though the regional differences of time mean properties do occur, regional mean time series of the properties have little differences regardless of the paramerization of the gas exchange rate. The little differences in the air-sea carbon fluxes may because of the compensation between the gas exchange rate (G) and the $(pCO_2^{ocn} - pCO_2^{atm})$ (or ΔpCO_2) contributions.

If we take the time mean of the regional average of F_{CO2}, pCO_2, and G, we can investigate the compensation quantitatively. All three simulations in both regions have negative values for mean F_{CO2} (uptake). In Antarctic region, the average carbon uptake in

hoQ (hoC) run is 2.5% (4.4%) smaller than that of control run, while in Subantarctic region, the uptake in hoQ (hoC) run is 5.8% (7.9%) smaller than that of control run. These values show little differences between the three simulations, with slightly larger differences in Subantarctic region. Having the time mean values of the regional average pCO_2^{atm} about 380 μatm in both regions, the hoQ (hoC) run has a 56.6% (90.9%) larger negative value of ΔpCO_2 comparing to the control run in the Antarctic region. In the Subantarctic region, the hoQ (hoC) run has a 33.6% (45.5%) larger negative value of ΔpCO_2 comparing to the control run. Moreover, the hoQ (hoC) run has a 14.8% (13%) smaller value of G in the Antarctic region, while the hoQ (hoC) run has a 14.8% (20.9%) smaller value of G comparing to the control run in the Subantarctic region. Therefore, we can conclude that during our simulation period and in the SO region we investigated, a larger difference between air and sea pCO_2 accompanies a smaller G value. Therefore, the variability of G and ΔpCO_2 compensates each other, leading to little differences of F_{CO2} in the three simulations.

Furthermore, we can tell that the variability of pCO_2 strongly impact that of F_{CO2}. Bearing in mind that the variability of G only contributes to the magnitudes of F_{CO2} but not the signs, we would like to understand more of the seasonal cycle of pCO_2. Figure 3.8 shows the seasonal cycle of zonal mean ΔpCO_2 from about 35°S to 65°S. Figure 3.8 (a) shows the observational ΔpCO_2 from Takahashi climatology, and figure 3.8 (b) shows the same variable as (a) but is based on our SOSE-OCMIP simulation model. We can see postive ΔpCO_2 during late winter to spring in the Antarctic region in both Takahashi observation and our simulation. Moreover, negative ΔpCO_2 occurs in the Subantarctic region around about 45°S, and persists for all seasons in observation, but happens only during fall to spring and with much smaller magnitudes in our simulation. The largest difference between the Takahashi observation and our simulation is around 35°S, where ΔpCO_2 shows positive values in our simulation during the austral summer, while it shows

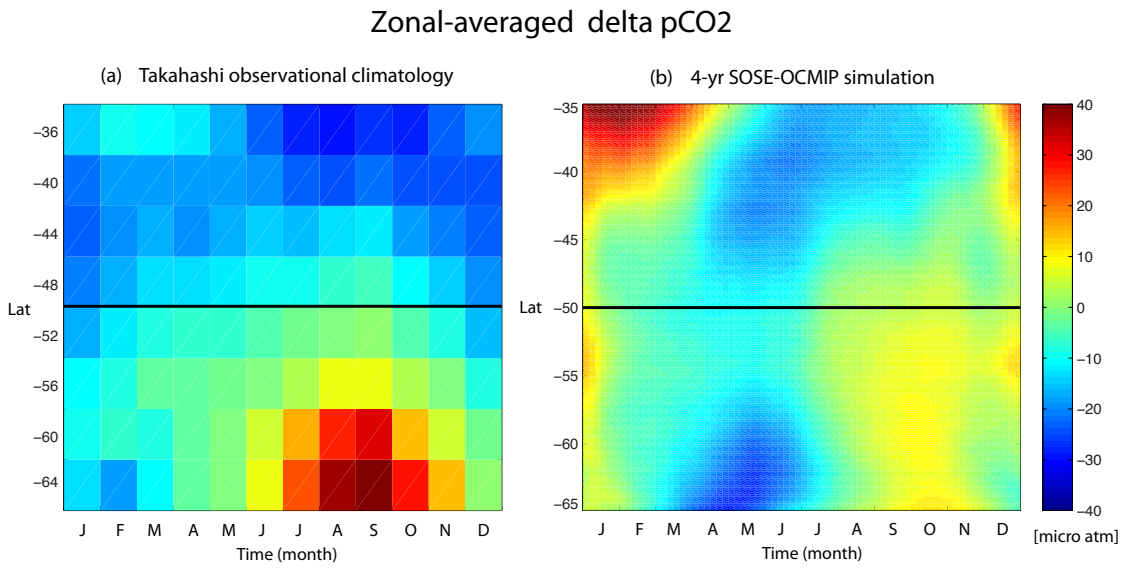

Figure 3-8: The seasonal cycle of zonal mean delta pCO_2 in a latitudinal range of about 65°S to 35°S. (a) shows the observational data from Takahashi monthly climatology (http://www.ldeo.columbia.edu/res/pi/CO2/carbondioxide), and (b) shows the simulation results from our SOSE-OCMIP model

negative values all over the seasons in observation. Although the differences between Takahashi observation and our model simulation can be seen in figure 3.8, we have to note that while we used the year 2005 to 2008 as our simulation period, the Takahashi climatology has a reference year of 2000. Moreover, while the model has a better spatial resolution than observation, our simulations only have a four-year time period. To further investigate the variability of oceanic pCO_2 and thus of ΔpCO_2 in seasonal to interannual timescales, we would like to investigate the drivers of the variability of pCO_2.

3.1.3 Controllers of the variability of partial pressure of carbon dioxide

For calculating the components that mainly controls the variability of the oceanic pCO_2, we used the linearization of carbonate chemistry. (Woloszyn et al., 2011, Follows et al., 2006) We linearized carbonate chemistry based on the work of Woloszyn et al. (2011) to compute the regional contributions from temperature (T), salinity (S), dissolved

inorganic carbon (DIC), and alkalinity (Alk) to oceanic pCO_2. Note that we normalized DIC and Alk with salinity to isolate the freshwater effect. In order to get the sensitivities of pCO_2 on T, S, DIC and Alk, we utilized the subroutine in Follows et al. (2006). We calculated the time mean values for the reference states. Moreover, we adjusted the nutrient concentration equations to fit the SO conditions: We regressed PO_4 and SiO_2 onto (salinity/35) based on the World Ocean Atlas monthly climatology (WOA09) for the Subantarctic region. In the Antarctic region, we used constant values for phosphate and silicate concentration (45mmolm^{-3} for silicate and 2.2mmolm^{-3} for phosphate.) The result is shown in figure 3.9. The reference value of pCO_2 is the time mean of the regional pCO_2 magnitudes, which is 377.7 µatm in the Antarctic region, and 376.2 µatm in the Subantarctic region.

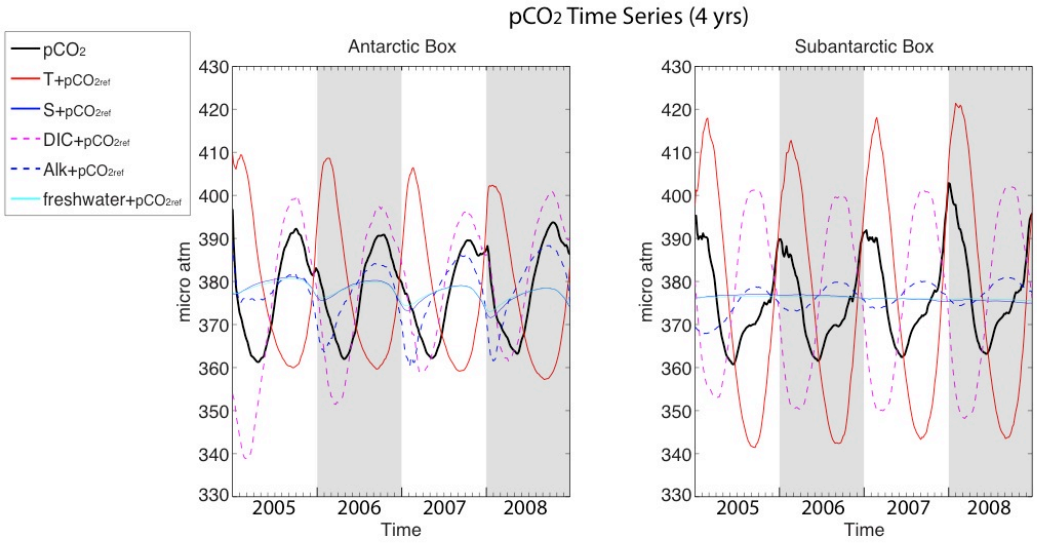

Figure 3-9: The time variability of regional oceanic pCO_2 and other variables (temperature, salinity, dissolved inorganic carbon, alkalinity, and freshwater effects) that contribute to the variability of pCO_2. Note that we added the regional time-mean pCO_2 to all time series of other variables to compare to the time series of pCO_2

The dominant controls of pCO_2 differ in the Antarctic and the Subantarctic regions. The variability of pCO_2 in the Antarctic region is dominated by the variability of

DIC. Both DIC and Alk variability are in phase with the variability of pCO_2 in this region, but the temperature contribution, which plays a secondary role, is out of phase with pCO_2. Note that the interannual variability of temperature moderates that of DIC. Moreover, the seasonal variability of Alk, though in phase with that of pCO_2, has smaller contribution to pCO_2 variability than that of DIC.

In the Subantratic box, the interannual variability of DIC plays a much smaller role. The seasonal cycle of temperature, which is the main controller of the pCO_2 variability, is much larger in this region comparing to that in Antarctic region. The seasonal variability of DIC is clearly out of phase with that of pCO_2 and temperature. The variability of pCO_2 is dominated by both seasonal and interannual variability of temperature, with a secondary modulation by the variability of DIC. Furthermore, both Alk and freshwater effects have negligible effects comparing to DIC and temperature contributions.

We conclude that the variability of temperature and DIC are the two main drivers of regional pCO_2 variance, controlling the air-sea carbon flux in the SO. The variability of temperature is relatively understood, especially on seasonal timescales. Thus, we focused on the variability of DIC in the following sections.

3.2 Regional Carbon Budget in the Southern Ocean

Considering the air-sea carbon fluxes, we can similarly separate the SO region into two regions: the Antarctic and the Subantarctic regions. We first establish the surface DIC budget in these regions before diagnosing the variability of DIC (Figure 3.10). Entrainment of high DIC water contributes to a CO_2 outgassing region in higher latitudes (the Antarctic region), while the surface cooling, subduction of the water, as well as the biological carbon uptake all drive a CO_2 uptaking region in lower latitudes (the Subantarctic region). Therefore, it is valuable to investigate the relative roles of ocean

transport, biological uptake, and the air-sea CO_2 flux in the SO in regulating the regional carbon budget.

Since the processes that governing atmosphere-ocean interaction in the SO region are rather complex, we analyzed the regional carbon budget based on the main activities such as oceanic carbon transport, biological carbon uptake, precipitation effect, etc. To

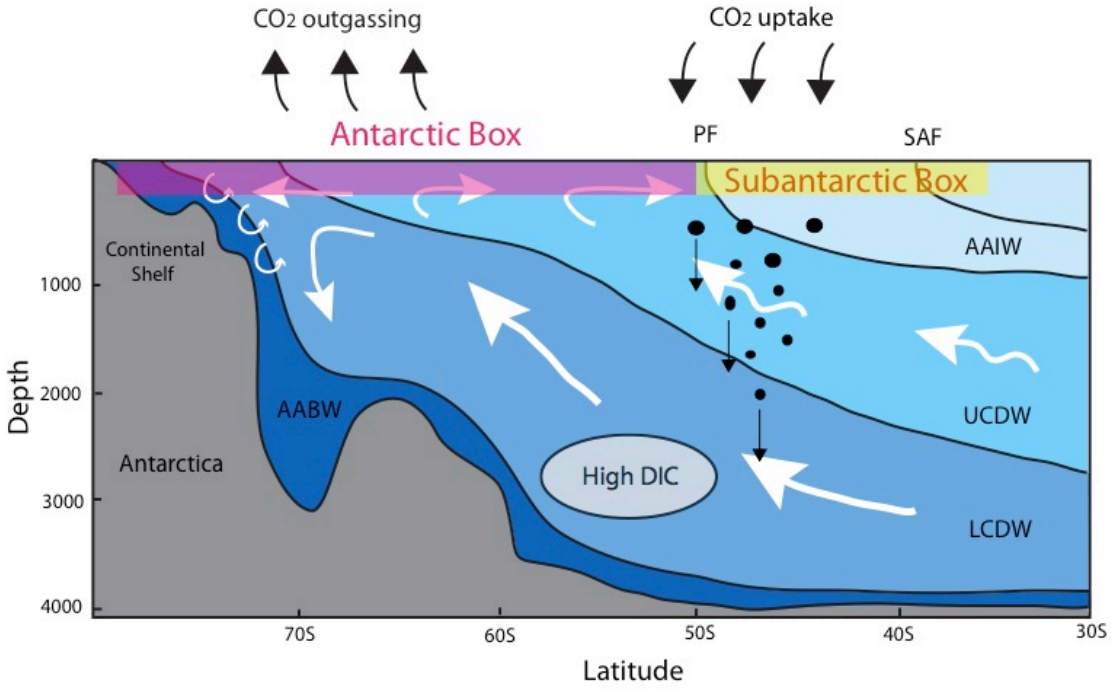

Figure 3-10: An illustration of the SO region carbon budget. The pink and yellow shading show the Antarctic and Subantarctic box from surface to about 250 meter deep. The white arrows represent the carbon transport by physical circulation, and the black arrows above the ocean box represent the regional air-sea carbon dioxide flux. The black dots in the subsurface Subantarctic region show the biological carbon uptake.

demonstrate the SO carbon budget quantitatively, we first expressed the carbon budget locally as:

$$\frac{\partial C}{\partial t} + \tilde{u} \cdot \nabla C = -\nabla \cdot \tilde{F} - \frac{F_{CO_2}}{\Delta Z_1} - B + \frac{C}{\Delta Z_1}(E - P),$$

(1) (2) (3) (4) (5) (6)

Where the local carbon time variance (1) is contributed by resolved circulation (2), sub-scale flux (3), air-sea exchange flux (4), biological uptake (5), and precipitation effect (6). Since we would like to investigate the regional carbon budget, we integrated the equation over the control volumes of the Antarctic and the Subantarctic sectors. Therefore, the regional carbon budget can be expressed as:

$$\frac{\partial}{\partial t}\iiint CdV = -\iint (\tilde{u}C)\cdot d\tilde{A} - \iint \tilde{F}\cdot d\tilde{A} - \iint_{z=0} F_{CO2}\cdot dA - \iiint BdV + \iint_{z=0} C(E-P)dA.$$

In order to completely close the regional carbon budget, we considered the free surface effect when calculating the change of DIC concentration with time. Note that for regional budget calculations, we only considered surface to 250 meter deep (figure 3.2).

We plot the mean seasonal cycle (Figure 3.11) and analyzed the regional carbon budget quantitatively. dCdt, which is the change of DIC with time, shows positive (DIC increases) values during the austral winter seasons and negative (DIC decreases) values during the summer seasons in both Antarctic and Subantarctic regions. Both biological uptake and transport play important roles in regional carbon budget in the seasonal time scale. In both Antarctic and Subantarctic regions, biological uptake mainly drives the DIC variability in austral summer, while transport mainly drives the DIC variability in austral winter. The transport of carbon is strongly related to the surface wind stress. The zonal wind stress at 50°S (30°S) is correlated with the upwelling (subduction) in the Antartic (Subantarctic) box with a coefficient of 0.93 (0.85). The merdional advection at 50°S (30°S) is correlated with the zonal wind stress at the same latitude with a coefficient of 0.97 (0.96). While the effect of precipitation contributes to little of the DIC variability, it is important during the austral summer in Antarctic region. Baring in mind the importance of the drivers of seasonal variability of DIC such as transport and biological carbon uptake, we would like to diagnose the variability of air-sea flux.

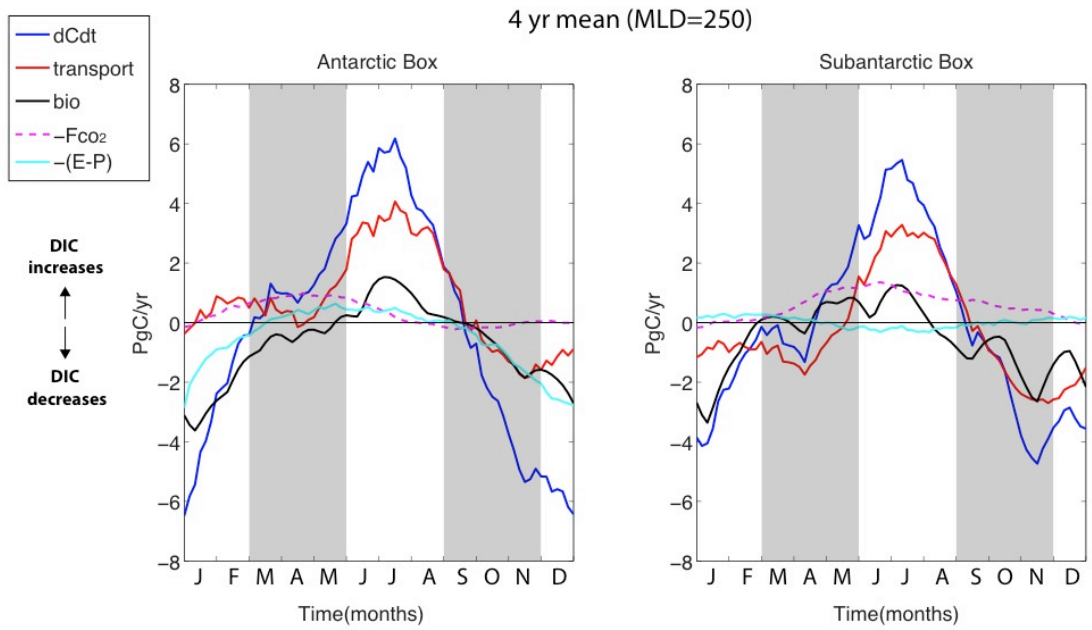

Figure 3-11: The four-year mean seasonal cycle of the change of dissolved inorganic carbon (DIC) with time, and other processes that contribute to the change of DIC. The change of DIC with time is shown in the blue lines. A positive (negative) value corresponds to an increase (decrease) in DIC concentration. The red lines represent the contribution of carbon transport, the black lines represent that of biological uptake, the pink dashed lines represent that of negative air-sea flux (a positive value represents an oceanic uptake of carbon dioxide), and the light blue lines represent that of the precipitation effect

3.3 The Seasonal Cycle of Air-sea Carbon Flux in Regional Differences

Both figure 3.11 and figure 3.5 show that the maximum air-sea carbon flux (uptake) happens during fall (MAM) in the Antarctic region, during later fall to winter (MAM to JJA) in the Subantarctic region. Note that we plot the negative air-sea carbon flux in figure 3.11. Therefore, a positive value for $-F_{CO2}$ represents an oceanic uptake flux of CO_2 from the atmosphere into the ocean. In this section, we further separate the time into four seasons, and show the variability in spatial maps instead of regional-mean values. We investigated the relationship of the seasonal variability of the air-sea carbon flux and that of pCO_2, and connected the carbon flux variability to other variances such as temperature and DIC that contribute to the variability of pCO_2.

We can illustrate the relationship between the seasonal cycle of the SO carbon budget and air-sea CO2 flux in Figure 3.12, Figure 3.13, and Figure 3.14. We analysis the seasonality by four seasons: DJF, MAM, JJA, and SON, which are austral summer, fall, winter, and spring, respectively. We can see a strong seasonality in pCO_2. A minimum of pCO_2 occurs during MAM (austral fall) in Antarctic region, while it occurs during MAM

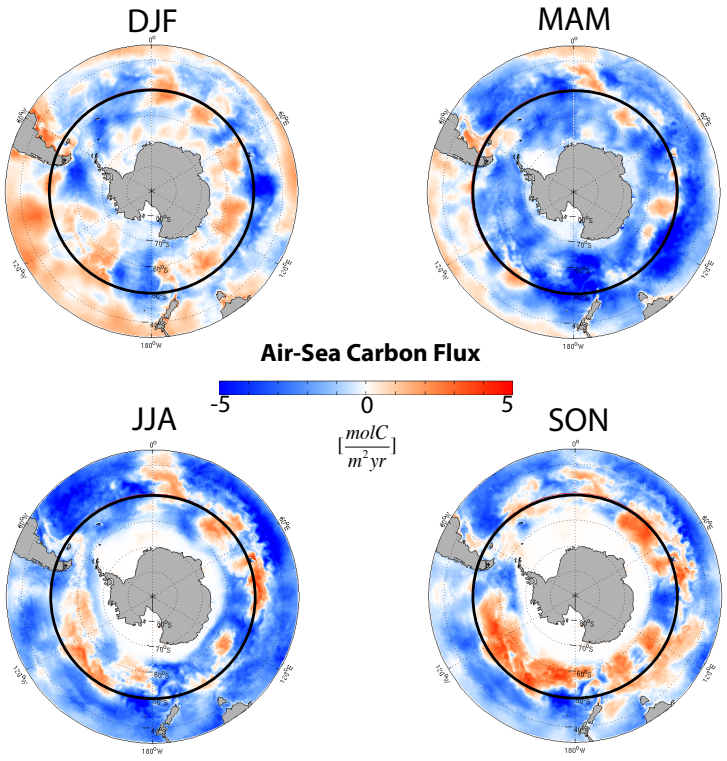

Figure 3-12: The spatial variability of the seasonal mean of air-sea carbon flux

to JJA (austral fall to winter) in Subantarctic region. These pCO_2 minimums are driven by the compensation of large anomalies in temperature and DIC during late summer, especially in Antarctic region (figure 3.9). During austral summer, biological carbon uptake drove down the surface layer carbon concentration, inducing a minimum in oceanic pCO_2 as shown in figure 3.11 and 3.9. Since the sea surface temperature is largest during summer, the summer minimum of pCO_2 is compensated by the minimum solubility. In Antarctic region, during late winter, Alkalinity has a negative contribution,

which further decreases the pCO_2 concentrations. Nevertheless, the Alk contribution is not important in Subantarctic region. It is the contribution of decreasing temperature during austral fall to winter that decreases the pCO_2 concentration in Subantarctic region during that time (figure 3.9).

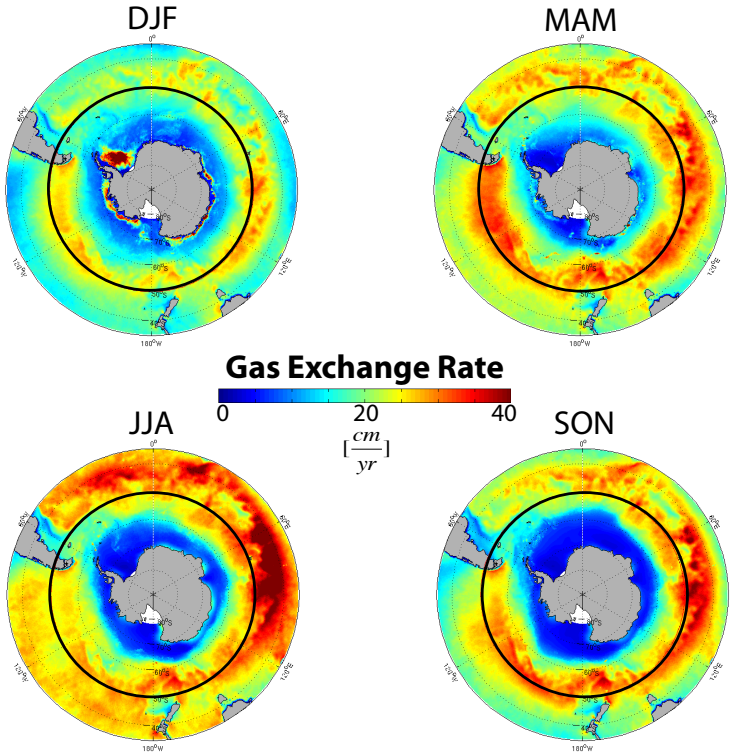

Figure 3-13: The spatial variability of the seasonal mean of gas exchange rate

Moreover, the maximum pCO_2 happens during austral summer in Subantarctic region, and during spring in Antarctic region. The main drivers of these maximum are summer high temperature and spring high-level DIC, which is contributed from wintertime maximum carbon transport into the SO region (figure 3.11). The seasonal patterns of air-sea carbon flux are similar to those of pCO_2, with smaller values of fluxes in the high latitudes because of the small gas exchange rates (figure 3.12, 3.13 and 3.14). In other words, the maximum uptake regions occur during MAM in Antarctic sector, and during MAM to JJA in Subantarctic sector, while the maximum outgassing happens

during SON in Antarctic sector, and during DJF in Subantarctic sector. These seasonal patterns are also shown in figure 3.5 and 3.11. However, the seasonal outgassing in both sectors is not obvious when we only consider the regional mean values (figure 3.11).

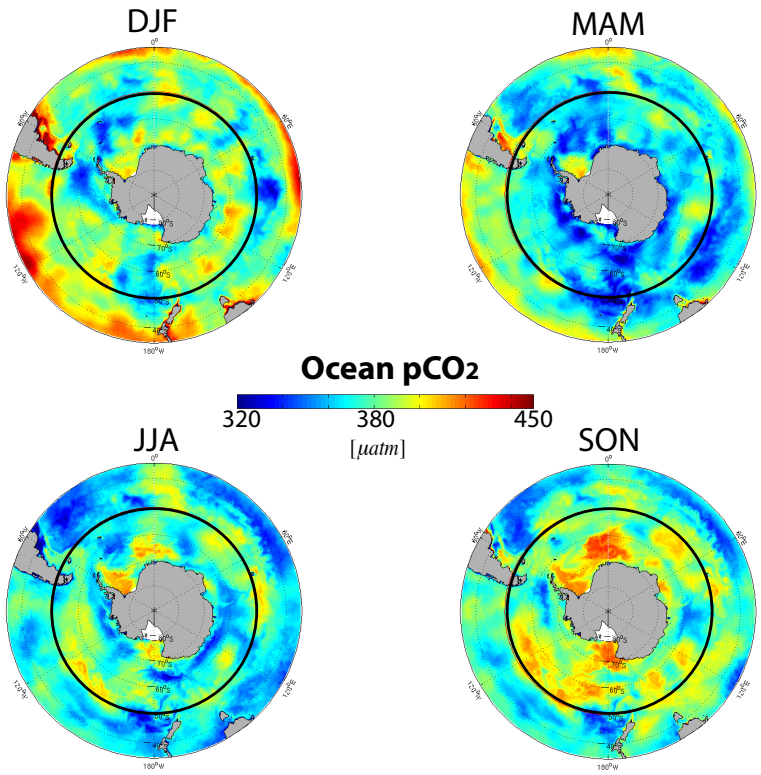

Figure 3-14: The spatial variability of the seasonal mean of oceanic partial pressure of carbon dioxide

3.4 Summary

According to the above discussion, the air-sea carbon flux in the SO region depends on both oceanic partial pressure of carbon dioxide (pCO_2) and gas exchange rate (G). While G (always positive) only contributes to the magnitude of the flux, pCO_2 influence both the sign and value of the flux. If we consider only the contribution of G, since the magnitude of G depends on both temperature and wind speed, the values of G

(and thus the contribution to the values of F_{CO_2}) are small in high latitudes and larger in the mid- and lower latitudes. Note that the regional variability is largest during JJA.

The contribution of pCO_2 to the variability F_{CO_2} is more complicated. Based on the linear decomposition of the carbonate chemistry (figure 3.8), the seasonal and interannual variability of pCO_2 is controlled by temperature, salinity, DIC, Alk, and freshwater effects. However, the contributions of these variables differ between the Antarctic and the Subantarctic regions. The variability of temperature is more dominant in the Subantarctic region, and the variability of DIC is more important in the Antarctic region. While both DIC and Alk are in phase with the variability of pCO_2 in the Antarctic region, the variability of temperature is out of phase with that of pCO_2. In the Subantarctic region, the variability of temperature is in phase with that of pCO_2, while DIC is out of phase with pCO_2. Furthermore, from the regional carbon budget analysis, we can know that the variability of DIC is mainly depends on the biological carbon uptake and the carbon transport into and out of the SO region. A schematic relationship between different variables and the SO air-sea carbon flux is shown in figure 3.15.

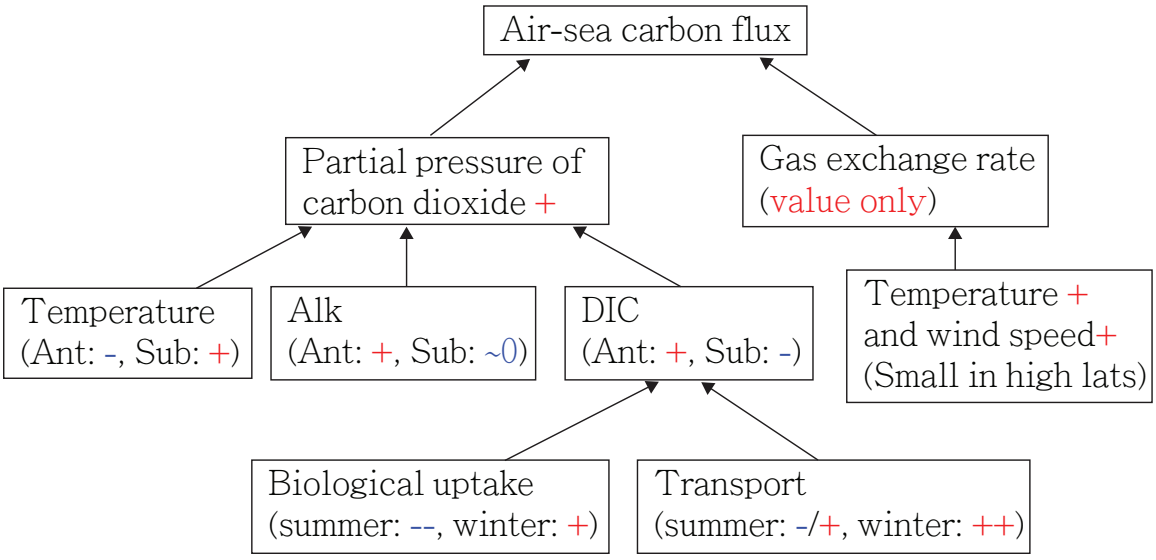

Figure 3-15: The relationship of the air-sea carbon flux in the SO region and different variables. + (-) represents positive (negative) contribution by the variable to the variability of the variable above it

CHAPTER 4

CONCLUSION

This study addresses the following questions: what controls the variability and the seasonal cycle of air-sea CO_2 flux in the SO? To answer this question, we performed several regional simulations of the carbon cycle in the SO and analyzed the processes controlling the air-sea carbon flux on seasonal to interannual timescales. The model is based on the offline biogeochemistry model (Ito et al., 2010; Woloszyn et al., 2011), in which we utilized the eddy-permitting circulation fields from the Southern Ocean State Estimate (Mazloff et al., 2010). The spatial pattern and the seasonal cycle of the air-sea carbon dioxide flux is calculated, and is broadly consistent with climatological observations (Takahashi et al., 2009). Furthermore, we also investigated the mechanisms underlying the air-sea flux.

The partial pressure of carbon dioxide in the surface water plays the dominant role in controlling the variability of air-sea carbon dioxide flux. The seasonal cycle of pCO_2 is in turn controlled by the compensating changes in temperature and dissolved inorganic carbon. The nature of compensation changes between the DIC-dominated Antarctic region and the temperature-dominated Subantarctic region.

Air-sea carbon flux reflects the strong seasonal variability of pCO_2. The lowest surface pCO_2 and the strongest carbon uptake occur during the fall in the Antarctic region, and between the fall and the winter in the Subantartic region. In contrast, the highest surface pCO_2 occurs during the spring in the Antarctic region, and the summer in the Subantarctic region. The maximum values of both pCO_2 and F_{CO2} are contributed by the combination of summer high temperature and spring high DIC. The thermal effect dominates in the Subantarctic region because of the larger seasonal temperature range. The DIC effect dominates the Antarctic region, which is mainly driven by the large

carbon transport during the winter seasons. For the fall-winter minimum pCO_2 values, the causes are slightly different between the Antarctic and the Subantarctic regions. It is the combination of DIC and Alk compensating with the temperature effect that contributes to the minimum values in the Antarctic region. In the Subantarctic region, the decrease of temperature during fall is the main driver. However, the compensation between temperature and DIC effects is also crucial to the minimum pCO_2 and F_{CO2} values there.

We also evaluated the dynamical adjustment of surface DIC and pCO_2 in response to the different gas exchange parameterization in the sensitivity experiments, in which several forms of the wind-speed dependence of the gas transfer coefficients are used. The analysis allows us to quantify the uncertainty arising from the parameterization of air-sea gas transfer. We conclude that specific choices of G have little impact on spatially integrated carbon flux. During our simulation period and in the SO region we investigated, a larger difference between air and sea pCO_2 accompanies a smaller G value. In other words, the contribution of the variability of G and ΔpCO_2 to the spatially integrated carbon flux compensates each other.

Model Improvement and Future Work

Our simulation well captured the SO carbon cycle variability on seasonal to interannual timescales. Moreover, the sensitivity tests of the gas exchange rate show that the effect of the parameterization of the air-sea transfer coefficient on the regional-integrated carbon fluxes is small. However, the model still contains several weaknesses and needs further improvement. For example, our current model cannot fully capture the biological variability because of the macro-nutrient restoring scheme. To improve the model, a more realistic scheme considering the nutrient cycle should be employed. The impact of iron cycling on the SO carbon cycle is also not taken into account in our model. The cycling of iron plays an important role regulating the SO productivity (Pollard et al., 2009; Coal et al., 2004; Boyd et al., 2000).

A possible direction of future research would be to perform a suite of dye simulations from hypothetical iron source regions, which include aerosol deposition, upwelling of deep water, and continental shelves, and to directly simulate the iron biogeochemistry (Parekh et al., 2005) by adding iron sources one at a time. In addition to the iron cycling on the SO carbon cycle, the ecosystem also plays an important role in this region, which can be simulated using an ecosystem-carbon cycle model including a representation of iron cycling and a few dominant phytoplankton functional groups (Dutkiewicz et al, 2009). Such models may allow us to diagnose the role of eddies in iron and carbon transport, and analysis the factors the limit the biological productivity in the model. Based on the outcome of the diagnostic study, we can further perform a few sensitivity experiments to test specific mechanisms controlling regional biological carbon uptake.

REFERENCES

Baker, D. F., et al., 2006: Transcom 3 inversion intercomparison: Impact of transport model errors on the interannual variability of regional CO2 fluxes. *Global Biogeochem. Cycles*, GB1002.

Bender, M.L. et al., 2005: Atmospheric O2/N2 changes, 1993–2002: Implications for the partitioning of fossil fuel CO2 sequestration the partitioning of fossil fuel CO2 sequestration. *Global Biogeochem. Cycles*, **19**, GB4017.

Boehme, L., M. P. Meredith, S. E. Thorpe, M. Biuw, and M. Fedak, 2008: Antarctic Circumpolar Current frontal system in the South Atlantic: Monitoring using merged Argo and animalborne sensor data. *J. Geophys. Res.*, **113**, C09012.

Böning, C. W., A. Dispert, M. Visbeck, S. R. Rintoul, and F. U. Schwarzkopf, 2008: The response of the Antarctic Circumpolar Current to recent climate change. Nat. Geosci., **1(12)**, 864–869.

Boyd, P. W. et al., 2000: A mesoscale phytoplankton bloom in the polar Southern Ocean stimulated by iron fertilization. *Nature*, **407**, 695–701.

Ciasto, L. M., and D. W. J. Thompson, 2008: Observations of large-scale ocean–atmosphere interaction in the Southern Hemisphere. *J. Climate,* **21**, 1244–1259.

Coale, K. H. et al., 2004: Southern Ocean Iron Enrichment Experiment: Carbon Cycling in High- and Low-Si Waters. *Science*, **304**, 408.

Dutkiewicz, S., M. J. Follows, and J. G. Bragg, 2009: Modeling the coupling of ocean ecology and biogeochemistry. *Global Biogeochem. Cycles*, **23** GB4017.

Farneti, R. and T. L. Delworth, 2010: The role of mesoscale eddies in the remote oceanic response to altered Southern Hemisphere winds. *J. Phys. Oceanogr.*, **40**, 2348-2354.

Follows, M. J., T. Ito, and S. Dutkiewicz, 2006: On the solution of the carbonate chemistry system in ocean biogeochemistry models. *Ocean Modelling*, **12**, 290-301.

Forget, G. and C. Wunsch, 2007: Estimated global hydrographic variability. *J. Phys. Oceanogr*., **37**, 1997–2008.

Forget, G., 2010: Mapping ocean observations in a dynamical framework: A 2004–06 ocean atlas. *J. Phys.Oceanogr*., **40**, 1201-1221.

Garcia H. E., Locarnini R. A., Boyer T. P. Antonov, J. I., Zweng M. M., Baranova O. K. and Johnson D. R., 2010: World Ocean Atlas 2009, Volume 4: Nutrients (phosphate, nitrate, silicate). S. Levitus, Ed. NOAA Atlas NESDIS 71, U.S. Government Printing Office, Washington, D.C., 398 pp.

Giering, R., and T. Kaminski, 1998: Recipes for adjoint code construction. *ACM Trans. Math. Software*, **24**, 437–474.

Gilbert, J. C., and C. Lemare´ chal, 1989: Some numerical experiments with variable-storage quasi-Newton algorithms. *Math. Program*., **45**, 407–435.

Gloor, M., N. Gruber, J. L. Sarmiento, C. L. Sabine, R. A. Feely, and C. Roedenbeck, 2003: A first estimate of present and pre-industrial air-sea CO2 fluxes patterns based on ocean interior carbon measurements and models. *Geophys. Res. Lett*., **30(1)**, 1010.

Gong, D. and Wang, S., 1998: Antarctic oscillation: comcept and applocations. *Chinese Sci. Bull.*, **43**, 734-738.

Gong, D. and S. Wang, 1999: Definition of Antarctic oscillation index. *Geophys. Res. Lett.*, **26**, 459-462.

Gould, J., and Coauthors, 2004: Argo profiling floats bring new era of in situ ocean observations. *Eos, Trans. Amer. Geophys. Union*, **85**.

Gruber, N., P. Friedlingstein, C. B. Field, R. Valentini, M. Heimann, J. E. Richey, P. Romero-Lankao, D. Schulze, and C. Chen, 2004: The vulnerability of the carbon cycle in the 21st century: An assessment of carbon-climate-human interactions, in *The Global Carbon Cycle: Integrating Humans, Climate, and the Natural World*, edited by C. B. Field and M. R. Raupach, chap. 2, pp. 45– 76, Island Press, Washington, D.C.

Gruber, N., et al., 2009: Oceanic sources, sinks, and transport of atmo- spheric CO2, *Global Biogeochem. Cycles*., **23**, GB1005.

Gupta, A. S. and M. H. England, 2006: Coupled ocean–atmosphere–ice response to variations in the southern annular mode, *J. Climate*, **19**, 4457-4486.

Gurney, K. R., et al, 2002: Towards robust regional estimates of CO2 sources and sinks using atmospheric transport models. *Nature*, **415**, 626–630.

Gurney, K. R., et al., 2003: TransCom 3 CO2 inversion intercomparison: 1. Annual mean control results and sensitivity to transport and prior flux information. *Tellus*, Ser. B., **55**, 555–579.

Gurney, K. R., et al., 2004: Transcom 3 inversion intercomparison: Model mean results for the estimation of seasonal carbon sources and sinks. *Global Biogeochem. Cycles*, **18**, GB1010.

Hall, A. and M. Visbeck, 2002: Synchronous variability in the Southern Hemisphere atmosphere, sea ice, and ocean resulting from the annular mode. *J. Climate,* **15**, 3043-3057.

Ho, D. T., et al., 2011: Toward a universal relationaship between wind speed and gas exchange: Gas transfer velocities measured with 3He/SF6 during the Southern Ocean Gas Exchange Experiment, *J. Geophys. Res*., **116**, C00F04.

Hofmann, M. and M. A. Morales Maqueda, 2011: The response of Southern Ocean eddies to increased midlatitude westerlies: A non-eddy resolving model study. *Geophys. Res. Lett.*, **38**, L03605.

Ito, T., M. Woloszyn, and M. Mazloff, 2010: Anthropogenic carbon dioxide transport in the southern ocean driven by Ekman flow. *Nature*, **463**, 80-83.

Jones, D. C., T. Ito, and N. S. Lovenduski, 2011: The transient response of the Southern Ocean pycnocline to changing atmospheric winds. *Geophys. Res. Lett.*, **38**, L15604.

Joos, F., G.-K. Plattner, T. F. Stocker, O. Marchal, and A. Schmittner, 1999b: Global warming and marine carbon cycle feedbacks on future atmospheric CO2. *Science*, **284**, 464–467.

Kalnay, E., and Coauthors, 1996: The NCEP/NCAR 40-Year Reanalysis Project. *Bull. Amer. Meteor. Soc*., **77**, 437–471.

Key, R.M., Kozyr, A., Sabine, C.L., Lee, K., Wanninkhof, R., Bullister, J.L., Feely, R.A., Millero, F.J., Mordy, C., Peng, T.H., 2004: A global ocean carbon climatology: results from Global Data Analysis Project (GLODAP). *Global Biogeochem. Cycles*, **18 (4)**, GB4031.

Khatiwala, S., F. Primeau, and T. Hall, 2009: Reconstruction of the history of anthropogenic CO2 concentrations in the ocean. *Nature*, **462(7271)**, 346–349.

Large, W. G., J. C. McWilliams, and S. C. Doney, 1994: Oceanic vertical mixing: A review and a model with a nonlocal boundary layer parameterization, *Rev. Geophys*., **32**, 363–403.

Large, W. G., and S. G. Yeager, 2004: Diurnal to decadal global forcing for ocean and sea-ice models: The data sets and flux climatologies. NCAR Tech. Rep. TN-4601STR, 112 pp.

Le Quéré, C., et al., 2007: Saturation of the Southern Ocean CO2 sink due to recent climate change. Science, **316**, 1735–1738.

Le Quéré, C., T. Takahashi, E.T. Buitenhuis, C. Rodenbeck, and S.C. Sutherland, 2010: Impact of climate change and variability on the global oceanic sink of CO2. *Global Biogeochem. Cycles*, **24**, GB4007.

Lenton, A., and R. J. Matear, 2007: Role of the Southern Annular Mode (SAM) in Southern Ocean CO2 uptake. *Global Biogeochem. Cycles*, **21**, GB2016.

Lovenduski, N. S., N. Gruber, S. C. Doney, and I. D. Lima, 2007: Enhanced CO2 outgassing in the Southern Ocean from a positive phase of the Southern Annular Mode. *Global Biogeochem. Cycles*, **21**, GB2026.

Lovenduski, N. S., N. Gruber, and S. C. Doney, 2008: Toward a mechanistic understanding of the decadal trends in the Southern Ocean carbon sink. *Global Biogeochem. Cycles*, **22**, GB3016.

Manning, A.C. and R.F. Keeling, 2006: Global oceanic and land biotic carbon sinks from the Scripps atmospheric oxygen flask sampling network. *Tellus,* **58B**, 95–116

Marini, C., C. rankignoul, and J. Mignot, 2010: Links between the southern annular mode and the Atlantic meridional overturning circulation in a climate model, *J. Climate*, **24**, 624-640.

Marshall, J., A. Adcroft, C. Hill, L. Perelman, and C. Heisey, 1997: A finite-volume, incompressible Navier Stokes model for studies of the ocean on parallel computers. *J. Geophysical Res*., **102(C3)**, 5753-5766.

Marshall, G. J., 2003: Trends in the southern annular mode from observations and reanalyses, *J. Climate*, **16**, 4134-4143.

Martin, J. H., G. A. Knauer, D. M. Karl, and W. W. Broenkow, 1987: VERTEX: Carbon cycling in the northeastern Pacific. *Deep Sea Res., Part I* , **34** , 267–285.

Matear, R. J., and A. C. Hirst, 1999: Climate change feedback on the future oceanic CO2 uptake. *Tellus*, Ser. B., **51**, 722–733.

Mazloff, M. R., P. Heimbach, and C. Wunsch, 2010: An Eddy-Permitting Southern Ocean State Estimate. *J. Phys. Oceanogr.*, **40(5)**, 880-899.

Meredith M. P. et al., 2012: Sensitivity of the overturning circulation in the Southern Ocean to decadal changes in wind forcing. *J. Climate*, **25**, 99–110.

McNeil, B. I., N. Metzl, R. M. Key, R. J. Matear, and A. Corbiere, 2007: An empirical estimate of the Southern Ocean air-sea CO2 flux. *Global Biogeochem. Cycles*, **21**, GB3011.

Mikaloff Fletcher et al., 2006: Inverse estimates of anthropogenic CO2 uptake, transport, and storage by the ocean. *Global Biogeochem. Cycles*, **20**, GB2002.

Mikaloff Fletcher, S. E., et al., 2007: Inverse estimates of the oceanic sources and sinks of natural CO2 and the implied oceanic transport. *Global Biogeochem. Cycles*, **21**, GB1010.

Najjar, R., J. Sarmiento, and J. R. Toggweiler, 1992: Downward transport and fate of organic matter in the ocean: simulations with a general circulation model. *Glob. Biogeochem. Cycles*, **6**, 45–76.

Parekh, P., M. J. Follows, and E. A. Boyle, 2005: Decoupling of iron and phosphate in the global ocean. *Global Biogeochem. Cycles*, **19**, GB2020.

Patra, P. K., et al., 2006: Sensitivity of inverse estimation of annual mean CO2 sources and sinks to ocean-only sites versus all-sites observational networks, *Geophys. Res. Lett.*, **33**, L05814.

Plattner, G.-K., F. Joos, T. F. Stocker, and O. Marchal, 2001: Feedback mechanisms and sensitivities of ocean carbon uptake under global warming. *Tellus*, Ser. B., **53**, 564–592.

Pollard, R. T. et al., 2009: Southern Ocean deep-water carbon export enhanced by natural iron fertilization. *Nature*, **457**, 577.

Ponte, R. M., C. Wunsch, and D. Stammer, 2007: Spatial mapping of time-variable errors in Jason-1 and TOPEX/Poseidon sea surface height measurements. *J. Atmos. Oceanic Technol*., **24**, 1078–1085.

Quay, P., R. Sommerup, T. Westby, J. Sutsman, and A. McNichol, 2003: Changes in the 13C/12C of dissolved inorganic carbon in the ocean as a tracer of anthropogenic CO2 uptake. *Global Biogeochem. Cycles*, **17(1)**, 1004.

Renwick, J. A., 2004: Trends in the Southern Hemisphere polar vortex in NCEP and ECMWF reanalyses. *Geophys. Res. Lett.*, **31**, L07209.

Sabine, C.L. et al., 2004: The oceanic sink for anthropogenic CO2. *Science*, **305**, 367–371.

Sarmiento, J. L., T. M. C. Hughes, R. J. Stouffer, and S. Manabe, 1998: Simulated response of the ocean carbon cycle to anthropogenic climate warming. *Nature*, **393**, 245–249.

Takahashi, T., et al., 2002: Global sea-air CO2 flux based on climatological surface ocean pCO2, and seasonal biological and temperature effects. *Deep Sea Res. II*, **49(9– 10)**, 1601– 1622.

Takahashi, T., et al., 2009: Climatological mean and decadal changes in surface ocean pCO2, and net sea-air CO2 flux over the global oceans. *Deep Sea Res. II*, **56**, 554–577.

Takahashi, T. et al., 2012: The changing carbon cycle in the Southern Ocean. *Oceanography*, **25(3)**, 26–37.

Thompson, D.W.J., and J.M. Wallace, 2000: Annular modes in the extratropical circulation. Part I: Month-to-month variability. *J. Climate*, **13**, 1000-1016.

Thompson, D.W.J., and S. Solomon, 2002: Interpretation of recent Southern Hemisphere climate change. *Science*, **296**, 895-899.

Visbeck, M., 2008: A station-based southern annular mode index from 1884 to 2005, *J. Climate*, **22**, 940-905.

Wang, S.,1992: Studies on the atmospheric centers of actions. *Report in State University of New York at Stony Brooks*, 32pp.

Wanninkhof, R.,1992: Relationship Between Wind Speed and Gas Exchange Over the Ocean. *J. Geophys. Res.*, **97**, NO. C5, 7373-7382.

Woloszyn, M., M. Mazloff, and T. Ito, 2011: Testing an eddy-permitting model of the Southern Ocean carbon cycle against observations. *Ocean Modelling*, **39**, 170-182.

Wunsch, C. and P. Heimbach, 2007: Practical global oceanic state estimation. *Physica D*, **230**, 197–208.

Yoshikawa, C., M. Kawamiya, T. Kato, Y. Yamanaka, and T. Matsuno, 2008: Geographical distribution of the feedback between future climate change and the carbon cycle. *J. Geophys. Res*., **113**, G03002.